JOURNAL OF THERMOPHYSICS AND HEAT TRANSFER
Vol. 24, No. 2, April–June 2010

Nanosphere Near-Field Radiative Heat-Exchange Analysis

Laurie Y. Carrillo* and Yildiz Bayazitoglu†
Rice University, Houston, Texas 77251

DOI: 10.2514/1.45620

A theoretical method for sphere-to-sphere radiative heat exchange is implemented for silica, lithium fluoride, and arsenic selenide nanospheres of equal and unequal radii. The method is extended to approximate a sphere-to-plane geometric configuration via an asymptotic method. The asymptotic method calls for an iterative process by which the radiative exchange is continuously calculated up to convergence while increasing one microsphere radius. These results are compared with previously published theoretical approximations and experimental data.

Nomenclature

b	=	Wein's displacement constant, 2.898×10^{-3} m · K
E	=	electric field, V/m
$\bar{G}_E$	=	electric dyadic Green function, 1/m
$\bar{G}_M$	=	magnetic dyadic Green function, 1/m
H	=	magnetic field, V/m
$\hbar$	=	Dirac constant, 1.055×10^{-34} J · s
$\mathbf{J}$	=	current density, A/m^2
k_b	=	Boltzmann constant, 1.381×10^{-23} J/K
r	=	point location, m
T	=	temperature, K
V	=	volume
δ	=	Dirac delta function, 1/m
δ_{lm}	=	Kronecker delta, unitless
ε_0	=	permittivity of a vacuum, 8.854×10^{-12} F/m
ε''	=	imaginary part of dielectric function, unitless
θ	=	mean energy of Planck oscillator, J
λ	=	wavelength in vacuum, m
μ_0	=	permeability of vacuum, $4\pi \times 10^{-7}$ H/m
ω	=	angular frequency, rad/s

Subscripts

i	=	first Cartesian component
j	=	second Cartesian component
max	=	maximum

I. Introduction

WHEN two bodies exchanging radiation at a dominant wavelength λ are at a distance λ apart or less, near-field radiation effects are observed. Since the separation distance is based on wavelength, it is also dependent on temperature, as described by Wein's displacement law. Wein's displacement law states that the dominant wavelength of radiative emission is inversely proportional to the temperature of the body according to the formula

$$\lambda_{\max} = \frac{b}{T} \tag{1}$$

Here, Wein's displacement constant b is equivalent to 2.898×10^{-3} m · K. As the temperature of the bodies increases, the dominant wavelengths of radiative exchange become shorter. This means that the near-field domination distance between the two bodies decreases as the temperature increases. Traditional radiative heat transfer equations that are used to describe typical macroscale heat exchange neglect near-field radiation. This is an accurate representation when the bodies are farther apart than λ, which is the case in most macroscopic situations. However, at the nanoscale, when radiative transfer often includes near-field effects, these equations are no longer applicable. The radiative exchange is underpredicted by traditional radiative heat transfer equations.

Discussion of the limits of the laws of macroscopic heat transfer was published in [1]. Recently, there has been significant interest and advancements in describing radiative exchange including near-field effects [1,2]. Near-field radiative exchange occurs because of evanescent waves. These waves occur at the boundary of the material but rapidly decay as the distance away from the boundary increases. When a second body is brought near enough to the first body such that the evanescent wave has not yet decayed, the evanescent wave can tunnel into the second body. This radiation tunneling phenomenon generates the near-field energy transfer. An editorial overview of micro/nanoscale radiative heat transfer work is conducted in [3]. The radiative transfer of two semi-infinite bodies at nanometric distances is investigated in [4]. Equations that define radiative heat transfer between two spherical nanoparticles assuming dipole point sources, electromagnetic energy density near a surface, and the near-field radiative transfer between two planar surfaces are covered in [1]. A solution for radiative exchange including near-field effects beyond the dipole approximation is developed for two spherical bodies by Narayanaswamy and Chen [5]. Also included is an application of this solution to calculate the exchange between two silica microspheres of equal radii. Results of this method are compared with experimental data in [6]. The fields are written in terms of dyadic Green's function (DGF). The fluctuation dissipation theorem (FDT) is used and covered in detail in [7–9]. A more in-depth look at DGFs is found in [10–12]. Bessel functions are used to express various equations mathematically. Details of Bessel functions are found in [13–15]. A look at the thermal emission and exchange among an ensemble of spheres is examined in [16].

In this paper the procedure presented by Narayanaswamy and Chen [5] is used. For verification purposes and to ensure that the procedure was being properly applied, the silica microsphere of the equal-radii case from [5] was duplicated. The next step was to look at additional cases that had not been investigated. The smaller nanoscale regime was investigated. It has been stated by [5] that this regime can be approximated adequately by the dipole approximation. We would expect the dipole approximation to yield approximately the same values as those presented here. A comparison of the two methods was done and included in the Results section. Results agree for most of the gap range. As the gap decreased for the range of radii of spheres investigated in this paper, the accuracy also seemed to decrease. The more rigorous procedure in [5] is used in this paper in order to attain increased accuracy in these lower gap ranges, as well as to gain increased familiarity with the method. The procedure in [5]

Received 25 May 2009; revision received 28 October 2009; accepted for publication 31 October 2009.

*Graduate Student, Department of Mechanical Engineering and Materials Science, Mail Stop 321, P.O. Box 1892. Student Member AIAA.

†Professor, Department of Mechanical Engineering and Materials Science, Mail Stop 321, P.O. Box 1892.

was also applied to spheres of unequal radii. In addition to silica, the authors investigated other materials in the sphere-to-sphere configuration. An analysis was also done of the sphere-to-plane geometric configuration. This paper presents the results using a new asymptotic method. This was done by taking the sphere-to-sphere case and calculating the radiative exchange iteratively. The radius of one sphere was iteratively increased with the radiative exchange recalculated each time. This process was continued until the value calculated did not change significantly. These results were compared with experimental results acquired by Narayanaswamy et al. [6]. Theoretical results were also presented in [6] but by a different method. In [6], the theoretically calculated sphere-to-sphere radiative exchange curve was fit to the experimental data by adjusting a multiplier and adding an adjusted constant. The asymptotic method results in this work more closely match the experimental data. The work presented in this paper is done to contribute to the understanding of near-field radiative exchange, which has applications in nanomanufacturing, near-field thermal photovoltaic devices, and nanostructure imaging [17].

II. Formulation

We aim to calculate the Poynting vector $E \times H$ from the electromagnetic wave fields E and H to determine the spectral radiative exchange between spheres. These electromagnetic wave fields deal directly with emission of thermal radiation. We can then integrate over the wavelength to produce the total radiative exchange between the spheres. The Poynting vector is given in [5] as

$$\langle E_{i\omega} H^*_{j\omega} \rangle = i\omega\mu_0 \int_V \mathrm{d}^3 r' \{ \bar{\bar{G}}_E(\mathbf{r}_1, \mathbf{r}, \omega) \bar{\bar{G}}^*_M(\mathbf{r}_1, \mathbf{r}', \omega) \langle \mathbf{J}_l(\mathbf{r}, \omega) \mathbf{J}^*_m(\mathbf{r}', \omega) \rangle \} \tag{2}$$

where $\bar{\bar{G}}_E(\mathbf{r}_1, \mathbf{r}, \omega)$ and $\bar{\bar{G}}_H(\mathbf{r}_1, \mathbf{r}, \omega)$ are the DGFs due to a source at $\mathbf{r}$. Here, an additional mathematical technique involving kernels called DGFs, which use second-rank dyad tensors, is incorporated. DGFs are covered in detail in [10–12]. The integration is performed over the entire volume V containing the source, μ_0 is the permeability of vacuum, and $\mathbf{J}(\mathbf{r}, \omega)$ is the Fourier component of fluctuating current. To deal with the phenomena of fluctuation, a statistical average must be included within the formulation. This is denoted as $\langle \cdot, \cdot \rangle$. The equation can be manipulated further by the application of the FDT developed by Rytov et al. [9]. This theorem states that the density matrix for thermal fluctuations can be expressed in terms of $\theta(\omega, T)$ or the mean energy of the quantum oscillator, where

$$\theta(\omega, T) = \hbar\omega / (\exp(\hbar\omega / k_b T) - 1) \tag{3}$$

There are several different forms of the FDT. The one used in this work is from [7], shown as follows:

$$\langle \mathbf{J}_l(\mathbf{r}, \omega) \mathbf{J}^*_m(\mathbf{r}', \omega) \rangle = \omega \varepsilon_0 \varepsilon''(\omega) \theta(\omega, T) \delta_{lm} \delta(\mathbf{r} - \mathbf{r}') \tag{4}$$

where $\varepsilon''(\omega)$ is the imaginary part of the dielectric function, and ε_0 is the permittivity of a vacuum. Details of this calculation process and applicable computational convergence analysis information are given in [5,10]. By substitution, the following can then be written:

$$\langle E_i(\mathbf{r}_1, \omega) H^*_j(\mathbf{r}_1, \omega) \rangle = \frac{i\varepsilon_o \varepsilon''(\omega) \mu_0 \omega^2 \theta(\omega, T)}{\pi} \int_V \mathrm{d}^3 r \{ (G_E(\mathbf{r}_1, \mathbf{r}, \omega) G^*_H(\mathbf{r}_1, \mathbf{r}', \omega))_{ij} \} \tag{5}$$

The Fourier component of the fluctuating electric and magnetic field at any point r_1 outside a volume containing the sources is given by [12] as

$$\mathbf{E}(\mathbf{r}_1, \omega) = i\omega\mu_0 \int_V \bar{\bar{G}}_E(\mathbf{r}_1, \mathbf{r}, \omega) \cdot \mathbf{J}(\mathbf{r}, \omega) \, \mathrm{d}^3 r \tag{6}$$

$$\mathbf{H}(\mathbf{r}_1, \omega) = \int_V \bar{\bar{G}}_H(\mathbf{r}_1, \mathbf{r}, \omega) \cdot \mathbf{J}(\mathbf{r}, \omega) \, \mathrm{d}^3 r \tag{7}$$

where $\bar{\bar{G}}_E(\mathbf{r}_1, \mathbf{r}, \omega)$ and $\bar{\bar{G}}_H(\mathbf{r}_1, \mathbf{r}, \omega)$ are the DGFs due to a source at $\mathbf{r}$.

III. Results

Figure 1 details a comparison between the dipole approximation of radiative transfer described by Joulain et al. [2] vs the rigorous method presented by Narayanaswamy and Chen in [5]. Based on these results, the calculated values agree as the gap increases. This seems to be true, due to the fact that as the gap increases, the dipole geometry is more closely duplicated. To maintain accuracy in the entire range of investigation, the more rigorous method in [5] was used in the remaining graphs.

Figure 2 shows the results calculated compared with published results from Narayanaswamy and Chen in [5]. This was done for microspheres from 1–25 μm at varying separation gaps. Radiative exchange power over temperature difference vs gap is plotted on a log–log graph. The data are plotted $T_A \rightarrow T_B$, as described in [5]. The radiative exchange between two microspheres is analyzed to validate

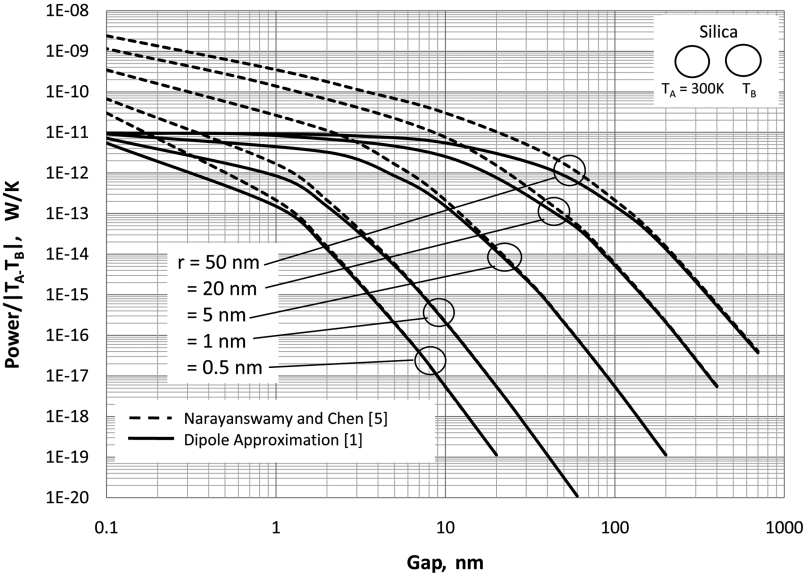

Fig. 1 Dipole approximation method in [1] vs the more rigorous method presented in [5].

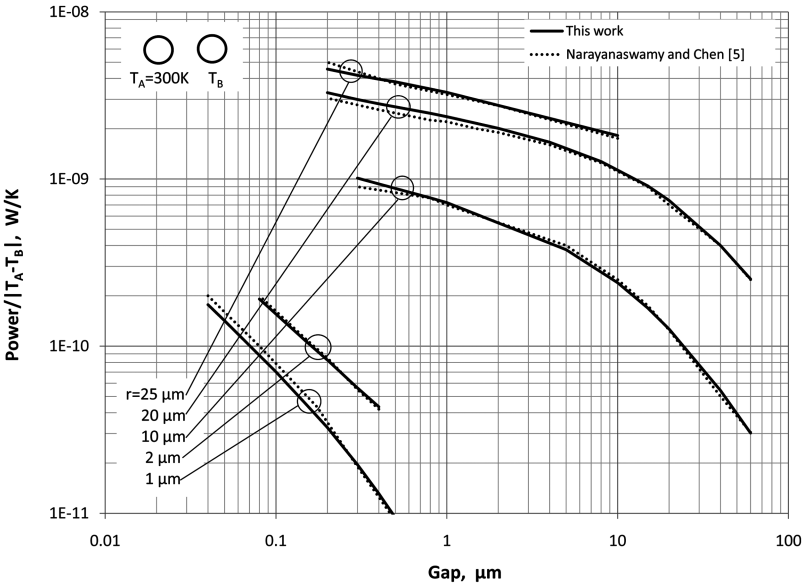

Fig. 2 Calculated vs published values for microscale silica spheres of equal radii.

that computational procedures produce results in a reasonable range, as with published data. The differences between the two results are due to the fact that graphical results and not exact numerical values were given in [5]. The authors estimated the numerical values by pulling points off the graph of [5] and plotting it with their results.

The radiative exchange between a 25 μm nanosphere and planar substrate are shown in Fig. 3. Note that the experimental data only include near-term radiative heat transfer and neglect far-field radiative effects. The far-field effects had to be subtracted from the total theoretical radiative exchange computed from the calculation process in this work. A best-fit line was acquired based on an equation containing a linear contribution proportional to the gap and a power contribution inversely proportional to the gap. The linear contribution representing the far-field effects was then subtracted. The dark line is the best-fit line corresponding to the experimental data from [6]. The dotted line is a curve acquired by taking the n from a best fit $y = Ax^{-n} + B$ curve for two 25 μm spheres and adjusting A and B to fit the experimental data. This procedure and data are presented in [6]. The mean error for this curve is 0.070 nW/K. The dotted line represents the asymptotic approach used to approximate the radiative exchange between the planar media and nanosphere. The results generated were acquired by beginning with two spheres at 25 μm. One of the spheres was slowly increased and the radiative exchange recalculated until convergence. Convergence was defined as $[(x_2 - x_1)/x_1] < 0.05$, where x_1 and x_2 represent two subsequent calculated results. The radius was increased to approximately 250 μm to reach the convergence criteria. For the cases tested, gap influenced the time it took for the results to be acquired but did not have a significant effect on when convergence was achieved. The mean error of the theoretical asymptotic approximation presented in this work is 0.032 nW/K. This is a 54% increase in the overall accuracy from the previously presented data when looking at the range from 3–10 μm. However, below 3 μm, the results generated by the asymptotic method in this paper are in agreement with those calculated by Narayanaswamy et al. [6].

Additional radiative exchange calculations for various nanosphere scenarios that have not been previously investigated were also analyzed. Additional configurations include radiative exchange between spheres of different temperatures, different materials, different radii ratios, and smaller nanosphere radii down to $r = 0.5$ nm. These

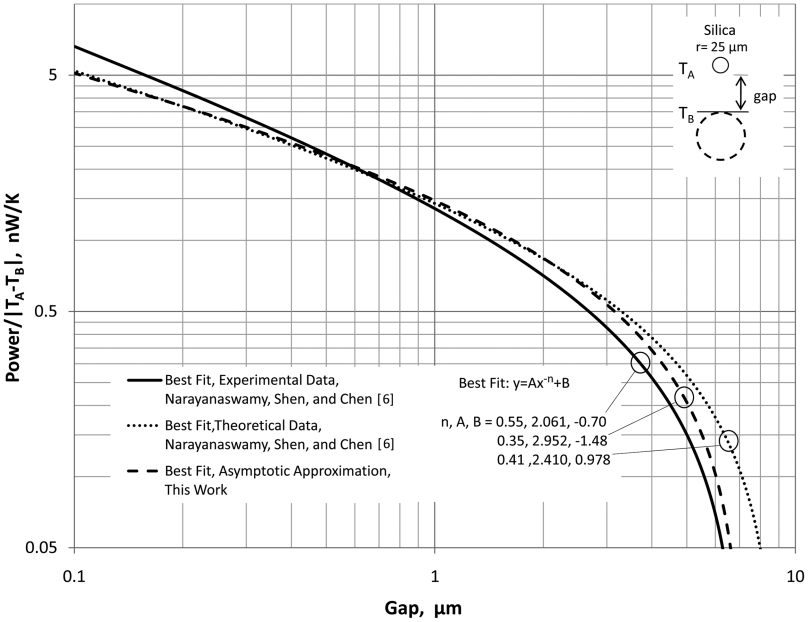

Fig. 3 Sphere-to-plane radiative exchange.

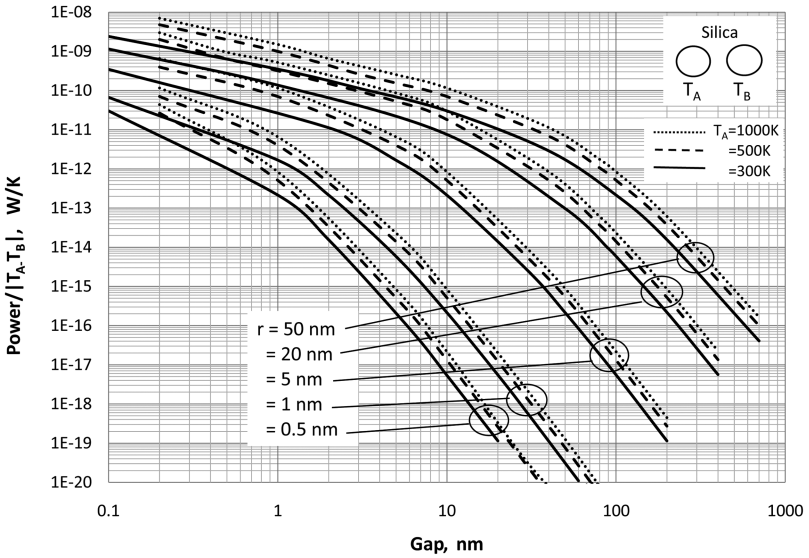

Fig. 4 Sphere-to-sphere radiative exchange: silica, equal radii, nanoscale.

graphs include both the effects of near-field and far-field exchanges. The results that follow represent these cases. Figure 4 shows results for the radiative exchange versus gap between two same-sized silica nanospheres. The range of radii is 50 to 0.5 nm. The temperatures included are for the cases of $T_A = 1000$, 500, and 300 K.

Several different materials were investigated for consideration of inclusion in thermal analysis. The primary material of investigation is amorphous silica, because experimental data, theoretical data, and resonant behavior of silica at the nanoscale are available in [5,6]. Additional materials considered for investigation were lithium niobate, sodium chloride, cubic carbon, arsenic triselenide-crystalline, silicon dioxide-alpha crystalline, titanium dioxide, potassium chloride, silicon monoxide, arsenic triselenide, silicon nitride, and lithium fluoride. The availability of data, technological applications, and feasibility toward analysis were assessed. Lithium niobate, arsenic triselenide-crystalline, silicon dioxide-alpha crystalline, and titanium dioxide have refractive indexes that varied with axis, making them difficult for analysis. The softness of sodium chloride makes its applications limited. The hardness of cubic carbon results in an unreasonable processing expense to create spherical geometries. Potassium chloride is hygroscopic, attracts water molecules, and therefore has limited applications. Data for silicon nitride and silicon monoxide had limited data available. Arsenic triselenide and lithium fluoride had available data at the frequency range of interest, refractive index data that did not vary with axis, and technological applications. For these reasons, these materials were also included in the analysis. Properties were taken from [18].

Figures 5 and 6 display calculated values similar to Fig. 4 but for lithium fluoride and arsenic triselenide. These results are for the temperature case of $T_A = 300$ K. The calculated values range from $1e-9$ to $1e-22$ W/K for arsenic triselenide, and from $1e-8$ to $1e-9$ for lithium fluoride. When comparing the material results in Figs. 4–6, lithium fluoride is shown to support the greatest degrees of radiative exchange, with the arsenic triselenide supporting the least. There is roughly a two-order-of-magnitude difference between the radiative exchange calculated for lithium fluoride than for the same configuration in arsenic triselenide.

Physically, the variations amongst materials can be understood by looking at a selection of spectral data for these materials. Figure 7 shows the resonance regions that occur within the spectral radiative power exchanged. The cases for each material were chosen such that the peaks would be approximately between $3e-11$ and $4e-11$ for plotting purposes. Note that for a gap of 10 nm, the arsenic triselenide sphere radius must be 20 nm to yield a peak in this range. Since the

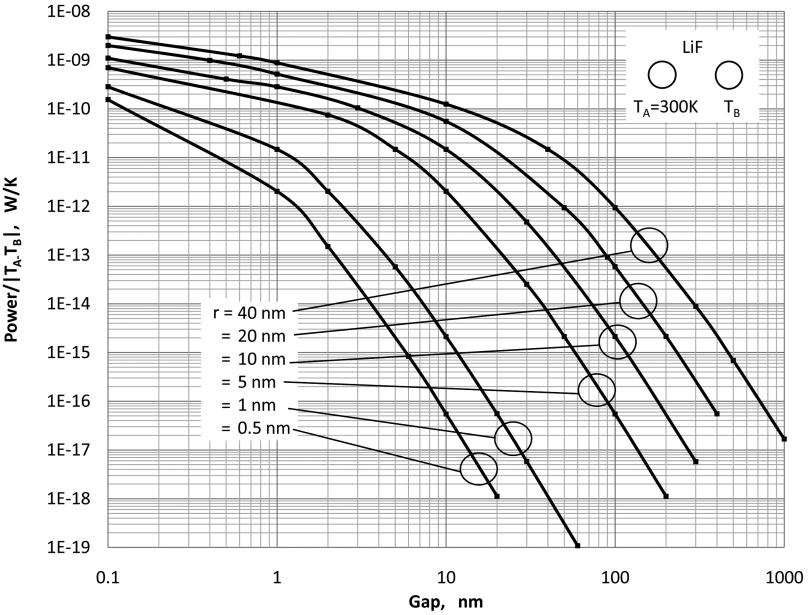

Fig. 5 Sphere-to-sphere radiative exchange: lithium fluoride, equal radii, nanoscale.

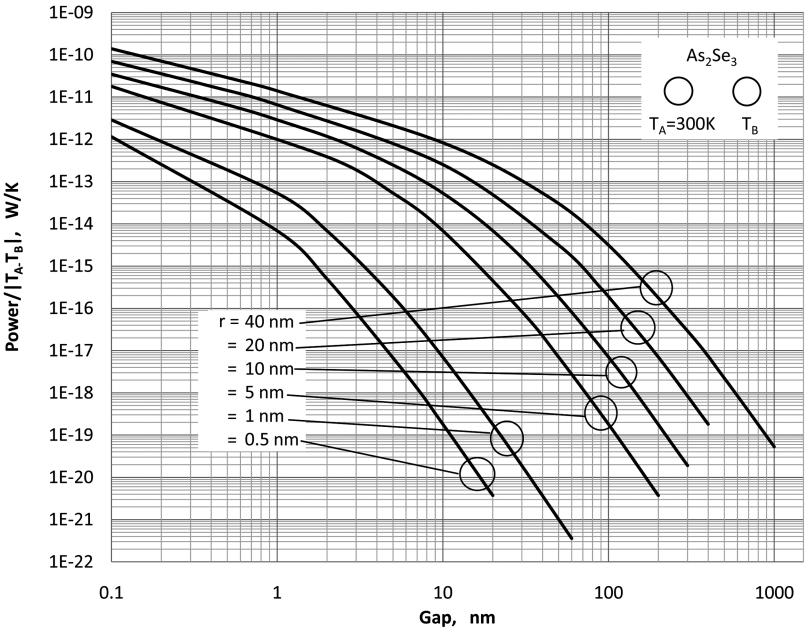

Fig. 6 Sphere-to-sphere radiative exchange: arsenic triselenide, equal radii, nanoscale.

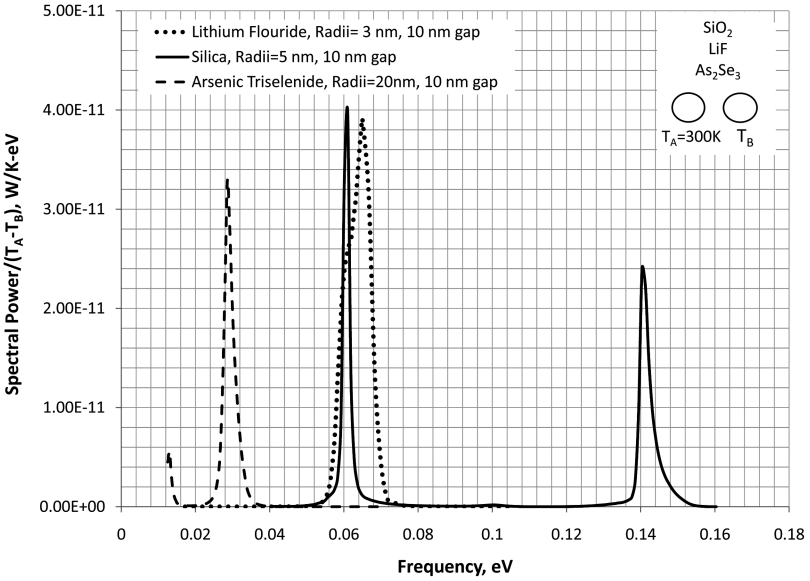

Fig. 7 Sphere-to-sphere spectral radiative exchange: various materials, equal radii, nanoscale.

resonant peak is much lower in arsenic triselenide for a given geometry compared with lithium fluoride and silica, it follows that the overall power will also be lower. Silica is unique in that it has two peaks. However, the width of the peak of the lithium fluoride is much thicker than silica, yielding a higher total power. In addition, the smaller sphere radii of 3 nm was required to plot the peak in the desired range, while silica required a radii of 5 nm. These resonant regions correspond to the refractive index: specifically, the imaginary component of the dielectric constant. Peaks occur within the dielectric constant at electron volts corresponding to the resonant peaks shown in the spectral plot.

The results shown in Fig. 8 depict the power over temperature difference calculated for two nanospheres of different radii at varying gap. These results are for the temperature case of $T_A = 300$ K. All three of the materials investigated are displayed. The higher degree of radiative exchange that exists in lithium fluoride is observed in this graph when the values are compared with the same configurations of silica and arsenic triselenide nanospheres. Results ranged from 1e − 18 to 1e − 11 W/K.

To further investigate the dependence of radiative exchange on radii ratio, calculations were done for the same radii ratio but with different individual nanosphere radii. These results are presented in Fig. 9. The radiative exchange is based on both radii of the spheres. There is a five-order-of-magnitude increase in the value for the exchange between 1 to 2 nm nanospheres and 10 to 20 nm nanospheres.

IV. Conclusions

An investigation of near-field radiative heat transfer was conducted. Two methods were calculated and then a comparison was plotted. The more complex method was used, for accuracy. The authors' results generated for silica sphere to silica sphere near-field transfer at the microscale agree with previously published data. Radii ratios, unequal spheres, and varied-temperature cases at the nanoscale were also examined. A new method for calculating sphere-to-plane radiative transfer was presented and results were shown to agree well with published theoretical and experimental data. The

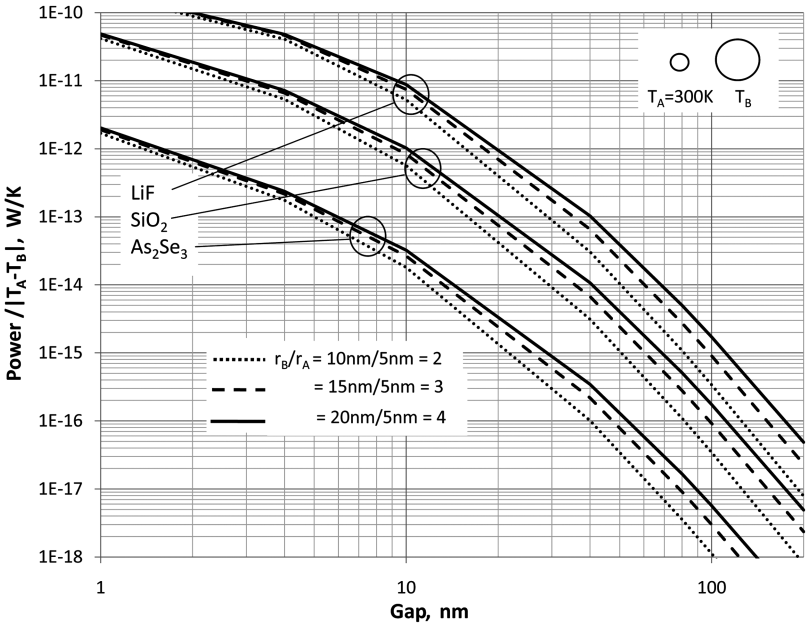

Fig. 8 Sphere-to-sphere radiative exchange: varying material, varying radii ratios, nanoscale.

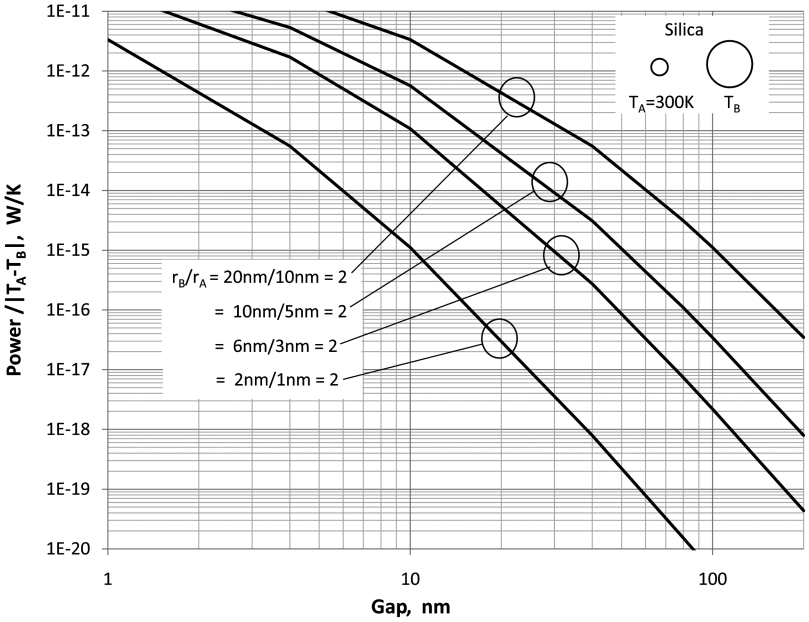

Fig. 9 Sphere-to-sphere radiative exchange: silica, radii ratio = 2, nanoscale.

spectral radiative transfer was investigated to understand the material's thermal performance.

References

[1] Volz, S. (ed.), *Microscale and Nanoscale Heat Transfer*, Topics in Applied Physics Series, Springer, Berlin, 2006, Chap. 1, pp. 4, 6. doi:10.1007/11767862

[2] Joulain, K., Mulet, J., Marquier, F., Carminati, R., and Greffet, J. J., "Surface Electromagnetic Waves Thermally Excited: Radiative Heat Transfer, Coherence Properties and Casimir Forces Revisited in the Near Field," *Surface Science Reports*, Vol. 57, No. 3–4, May 2005, pp. 59–112. doi:10.1016/j.surfrep.2004.12.002

[3] Zhang, Z., and Menguc, M. P., "Special Issue on Nano/Microscale Radiative Transfer," *Journal of Heat Transfer*, Vol. 129, No. 1, Jan. 2007, pp. 1–2. doi:10.1115/1.2401204

[4] Mulet, J., Joulain, K., Carminati, R., and Greffet, J., "Enhanced Radiative Heat Transfer at Nanometric Distances," *Nanoscale and Microscale Thermophysical Engineering*, Vol. 6, No. 3, July 2002, pp. 209–222. doi:10.1080/10893950290053321

[5] Narayanaswamy, A., and Chen, G., "Thermal Near-Field Radiative Transfer Between Two Spheres," *Physical Review B: Condensed Matter and Materials Physics*, Vol. 77, No. 7, 2008, Paper 075125. doi:10.1103/PhysRevB.77.075125

[6] Narayanaswamy, A., Shen, S., and Chen, G., "Near-Field Radiative Heat Transfer Between a Sphere and a Substrate," *Physical Review B: Condensed Matter and Materials Physics*, Vol. 78, No. 11, 2008, Paper 115303. doi:10.1103/PhysRevB.78.115303

[7] Landau, L. D., and Lifshitz, E. M., *Statistical Physics*, 3rd ed., Pt. 1, Reed Educational, Boston, 1985, pp. 386–393.

[8] Rytov, S. M., "Theory of Electric Fluctuations and Thermal Radiation," U. S. Air Force Cambridge Research Lab., Rept. AD0226765, Bedford, MA, July 1959.

[9] Rytov, S. M., Kravtsov, Y. A., and Tatarskii, V. I., *Principles of Statistical Radiophysics*, Vol. 3, Springer–Verlag, Berlin, 1989, pp. 109–122.

[10] Chew, W. C., *Waves and Fields in Inhomogeneous Media*, IEEE Press, Piscataway, NJ, 1995, pp. 15–16, 184–189, 375–428. doi:10.1163/156939393X00787

[11] Tsang, L., Kong, J. A., and Ding, K., *Scattering of Electromagnetic Waves: Theories and Application*, Wiley, Hoboken, NJ, 2000, pp. 54–60.

[12] Tai, C., *Dyadic Green's Function in Electromagnetic Theory*, 2nd ed., IEEE Press, Piscataway, NJ, 1994.

[13] Korenev, B. G., *Bessel Functions and Their Applications*, CRC Press, Boca Raton, FL, 2002, pp. 17–19.

[14] Abramowitz, M., and Stegun, I. A. (eds.), *Handbook of Mathematical Functions with Formulas, Graphs, and Mathematical Tables*, 9th ed., Dover, NY, 1972, pp. 435–478.

[15] Arfken, G., *Mathematical Methods for Physicists*, 3rd ed., Academic Press, Orlando, FL, 1985, pp. 633–634.

[16] Mackowski, D., and Mishchenko, M., "Prediction of Thermal Emission and Exchange Among Neighboring Wavelength-Sized Spheres," *Journal of Heat Transfer*, Vol. 130, Nov. 2008, Paper 112702. doi:10.1115/1.2957596

[17] Basu, S., Zhang, Z. M., and Fu, C. J., "Review of Near-Field Thermal Radiation and Its Application to Energy Conversion," *International Journal of Energy Research*, Vol. 33, No. 13, 2009, pp. 1203–1232. doi:10.1002/er.1607

[18] Palik, E. D., *Handbook of Optical Constants of Solids*, Academic Press, New York, 1985, pp. 623–798.